International Journal of Solids and Structures 50 (2013) 4226–4240

Contents lists available at ScienceDirect

International Journal of Solids and Structures

journal homepage: www.elsevier.com/locate/ijsolstr

Evaluation of a Statistically Equivalent Periodic Unit Cell for a quasi-periodic masonry

N. Cavalagli, F. Cluni *, V. Gusella

Department of Civil and Environmental Engineering, University of Perugia, Italy

ARTICLE INFO

Article history:
Received 4 January 2013
Received in revised form 5 July 2013
Available online 13 September 2013

Keywords:
Masonry
Quasi-periodic textures
Statistically Equivalent Periodic Unit Cell
Digital image processing
Periodic boundary conditions

ABSTRACT

The paper presents a method to estimate the Statistically Equivalent Periodic Unit Cell (SEPUC) corresponding to a masonry with quasi-periodic texture. The identification of the texture and the constituent phases (unit blocks and mortar joints) is achieved by means of digital image processing techniques applied to color image of the masonry wall. A statistical analysis of geometrical parameters (width and height of blocks, thickness and length of mortar joints) allows to estimate their probability distribution and to identify the typology of the texture. Subsequently a Monte Carlo analysis is performed using several tentative SEPUCs generated with different dimensions of blocks and joints according to the estimated distributions. A criterion was eventually proposed to identify, among the numerically generated ones, the SEPUC which is more suitable to model the behavior of masonry wall. The SEPUC is analyzed with techniques available for periodic texture, applying periodic boundary conditions, in order to estimate the equivalent elastic stiffness. The proposed method is validated comparing the results in the elastic range obtained with SEPUC and those obtained imposing essential and natural boundary conditions on the original texture.

1. Introduction

When dealing with the analysis of historical and monumental constructions, the engineer faces the challenge of estimating the mechanical characteristics of masonry. Moreover, very often the constituents of the masonry, blocks and mortar, are not arranged in a periodic pattern, where periodic means that blocks and mortar are placed in such a way that a cell may be identified within the texture which is capable of generating the whole masonry by means of pure translations. Nevertheless, in historical masonry very often a quasi-periodic texture is found, where quasi-periodic in this context means that rows of blocks with almost the same height can still be identified, even if the width of the stones inside each row and the height of different rows may vary. Therefore, it is very important to have models that can take into account the effective texture (i.e. the arrangement of blocks and joints) of historical masonry.

Considering the masonry with periodic texture, several methods are available in literature, developed starting from the work of Pande et al. (1989), with particular reference to the work of Anthoine (1995) which employed periodic boundary condition on a representative periodic cell.

Somewhat different methods must be used when dealing with masonry which have non-periodic texture. In particular, the concept of Representative Volume Element (RVE) is widely used. The RVE is defined as the cell for which the overall behavior (and therefore the elastic characteristics) is independent of the applied boundary conditions (Hill, 1963). It has been shown that, if the texture is ergodic, it is possible to consider only one sufficiently large domain subjected to boundary conditions in terms of stresses or displacements to estimate its mechanical characteristics (Sab, 1992). In Cluni and Gusella (2004) the homogenization was achieved by means of "test-windows" of increasing dimensions subjected to natural (i.e. in terms of stresses) and essential (i.e. in terms of displacements) boundary conditions until a mechanical convergence criterion was satisfied; moreover, the mechanical convergence criterion can be coupled with a statistical convergence criterion which take into account the most relevant information about the pattern (Gusella and Cluni, 2006). In a recent work (Cavalagli et al., 2011) this approach has been extended also to the estimation of the strength domain. Another approach for the estimation of the elastic characteristics of the non-periodic masonry which uses the texture derived from digital image processing is proposed in Lombardo et al. (2009).

For a quasi-periodic masonry, instead of the RVE, some form of "statistically equivalence" may be used to treat the masonry as a periodic medium. For example, the homogenized elastic characteristics may be estimated using a Statistically Equivalent Periodic

* Corresponding author. Tel.: +39 075 585 3955; fax: +39 075 585 3897.
E-mail addresses: cavalagli@strutture.unipg.it (N. Cavalagli), cluni@strutture.unipg.it (F. Cluni), guse@unipg.it (V. Gusella).

0020-7683/$ - see front matter © 2013 Elsevier Ltd. All rights reserved.
http://dx.doi.org/10.1016/j.ijsolstr.2013.08.027

Unit Cell (SEPUC), as in Šejnoha et al. (2008). In the case of non-linear behavior, it was shown in Sab (1994) that for Statistically Homogeneous Ergodic (SHE) media the results obtained in the case of periodic media are also valid. Besides natural and essential boundary conditions, periodic boundary conditions may be used in order to estimate the RVE of random media (Sab and Nedjar, 2005).

The main objective of the paper is the proposal of a new method to estimate the SEPUC of a masonry whose constituents (unit blocks and mortar joints) are arranged in a quasi-periodic pattern. The method takes into account the statistical description of the dimensions of the constituents (width and height of blocks, thickness and length of joints) and of their arrangement. The proposed method is based on the identification of texture and the generation of several tentative SEPUCs with dimensions of the constituents according to their probability distribution. A criterion based on the minimization of differences from mean values of statistical characteristics of the constituents and of concentration ratio is proposed to choose, among the others, the SEPUC of the masonry wall. The method is validated in the elastic range: in particular the SEPUC is analyzed with periodic boundary conditions and the results are compared to that obtained using the entire masonry wall subject to essential and natural boundary conditions.

The paper is written in the following sequence. In Section 2 a procedure based on algorithms available in digital image processing is proposed to obtain a consistent separation of the phases. In order to perform the statistical analysis the blocks are converted to equivalent rectangles and this allows to estimate the probability distributions of the dimensions of the constituents and their arrangement (texture) as described in Section 3. The statistical analysis allows to identify the periodic Statistically Equivalent Texture (SET) corresponding to the actual one, and several candidate SEPUCs are generated with different dimensions of the phase according to the their respective estimated probability functions. The choice of the SEPUC most suitable to model the masonry wall is made using a criterion which is presented in Section 4 with several alternatives. The proposed criterion is validated in Section 5 where the results obtained are compared to those which can be found by more consolidated approaches in the elastic range.

2. Digital image processing for the separation of phases

The first step in the procedure proposed in the present paper is the identification of stones and mortar joints and therefore to achieve a consistent separation of the phases starting from a color digital image of masonry. This can be achieved by means of Digital image processing (DIP) techniques (Gonzalez and Woods, 2002; Gonzalez et al., 2004).

In the present paper the procedure is used for two different masonries: the first one was also studied in Cavalagli et al. (2011), (indicated as masonry wall #1 in the following) and is shown in Fig. 1(a), while the second (indicated as masonry wall #2 in the following) is shown in Fig. 1(b).

A digital image can be described through functions $f(x,y)$ where x and y are the spatial coordinates of the pixel. The range of x is $0,1,\dots N-1$ and the range of y is $0,1,\dots M-1$, where N is the height of the image and M is the width of image, expressed in pixels. In the present cases, $N = M = 1500$.

A single image may be described by one ore more functions $f(x,y)$: for example, in a gray-scale image one function is sufficient, whose values are the gray levels, while a color image with RGB coding uses three functions f_R, f_G and f_B, whose values are the red (R), green (G) and blue (B) levels of the pixels.

In the following is presented the sequence of operation used to obtain the binary image from color image in the case of the masonry of Fig. 1(a); a similar procedure is used for masonry of Fig. 1(b).

The conversion from a color image represented by the vector of functions $\{f_R, f_G, f_B\}$ to a gray-scale image represented by function $g(x,y)$ is defined by the operator that calculate the value of luminance:

$$g(x,y) = 0.2989 \cdot f_R(x,y) + 0.5870 \cdot f_G(x,y) + 0.114 \cdot f_B(x,y) \tag{1}$$

The quality and definition of the image was improved using the median filter (Fig. 3(a)) which replaces the value of gray level of the pixel by the median of the gray levels on the surrounding pixels:

$$\bar{g}(x,y) = \text{median}\ \{g(s,t)\ \text{for}\ (s,t)\ \text{in}\ N_{(x,y)}\} \tag{2}$$

where $N_{(x,y)}$ is a square of side 3 pixels center in pixel at (x,y).

The gray-level image is then processed in order to separate the phases. In particular, noting that the histogram of gray levels (Fig. 2) has two dominant modes, the stones are identified as the "bright" portions of the image and the mortar as the "dark" portion.

Therefore the binary image (Fig. 3(b)) of the wall can be obtained with the following:

$$b(x,y) = \begin{cases} 0 & \text{if} \quad \bar{g}(x,y) \leqslant k \\ 1 & \text{if} \quad \bar{g}(x,y) > k \end{cases} \tag{3}$$

where k is the gray level used as a threshold (see Fig. 2). In the present case the value of the threshold level k is determined

(a) (b)

Fig. 1. Color image of the masonries analyzed: (a) masonry wall #1, (b) masonry wall #2.

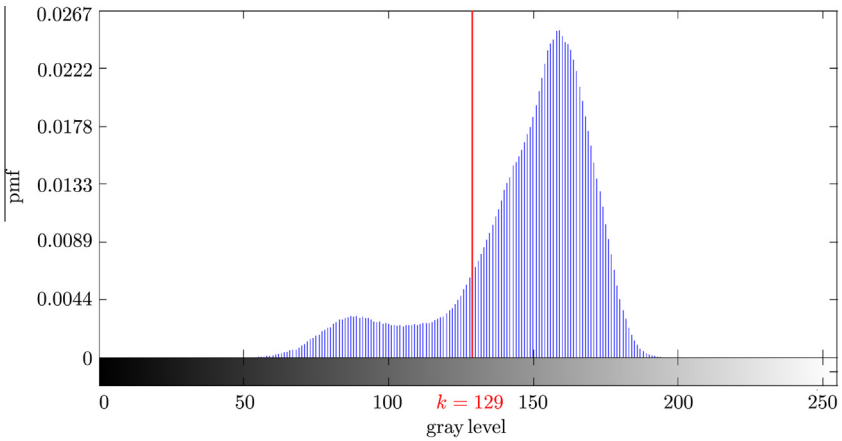

Fig. 2. Distribution of gray levels in the image of the masonry wall #1 in Fig. 1(a). The vertical line indicate the threshold used to separate phases: stones on the right, mortar on the left.

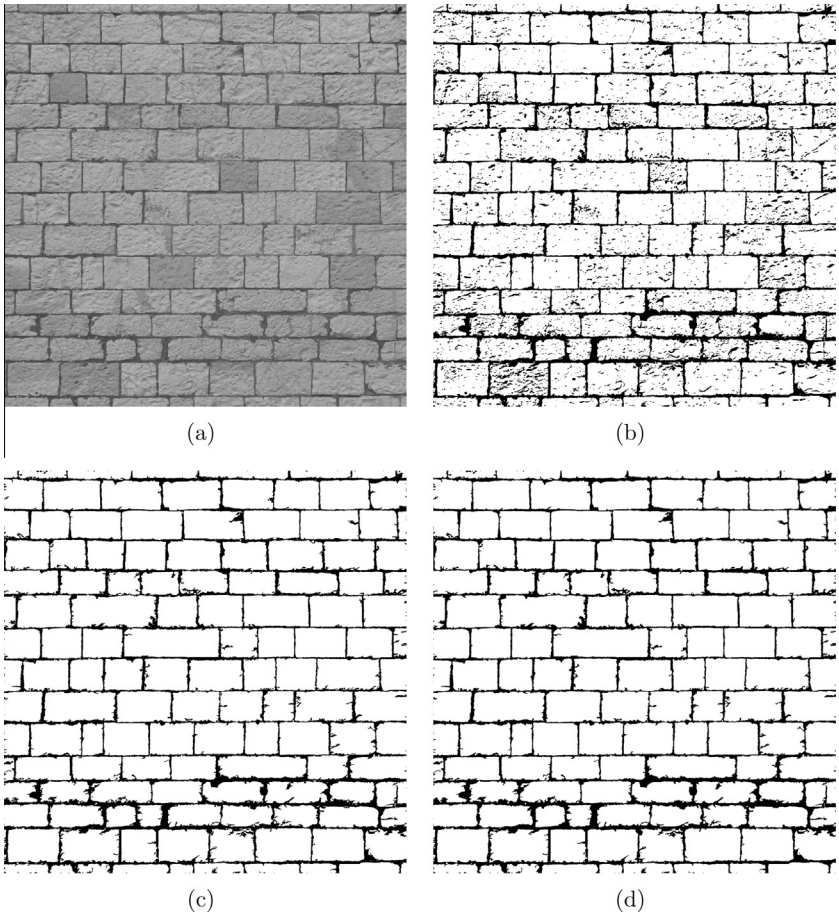

Fig. 3. Digital image processing of the image of masonry wall #1 (Fig. 1(a)): (a) conversion to gray-scale and application of median filter, (b) conversion to black and white, (c) filling of the holes, (d) erosion and dilatation.

through Otsu's method (for a detailed description see Gonzalez et al., 2004).

In the resulting binary image, the white portions (with value 1) are considered to be occupied by the stone phase, and the remaining black portion (with value 0) by the mortar phase.

Subsequently, morphological operators are used in order to enhance the quality of the separation of phases.

The use of morphological operator on black and white images is simplified if set operations are used. If $f(x,y)$ is the function which describes the black and white image, the same image can be seen as a set F: the relations which allow the passage from f to F and vice-versa are:

$$F = \{(x,y)|f(x,y) = 1\} \quad \text{and} \quad f(x,y) = \begin{cases} 1 & \text{if} \quad (x,y) \in F \\ 0 & \text{if} \quad (x,y) \notin F \end{cases} \tag{4}$$

Note that 1-valued pixels are said foreground pixels, while 0-valued pixels are said background pixels.

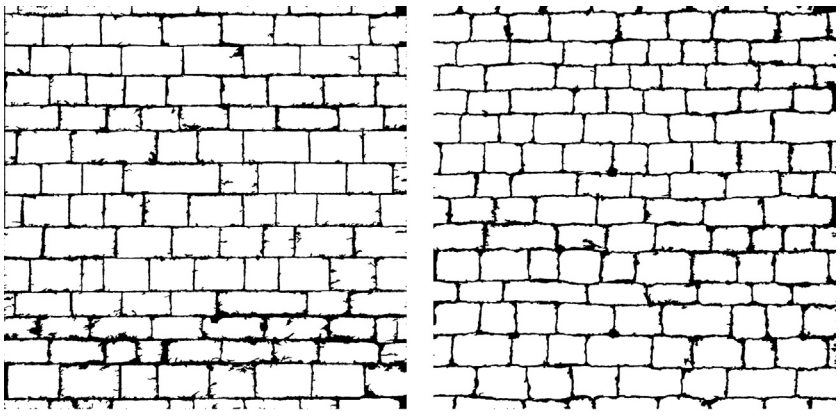

(a) (b)

Fig. 4. Binary images of the analyzed walls: (a) masonry wall #1 shown in Fig. 1(a), (b) masonry wall #2 shown in Fig. 1(b).

The usual operation on sets (union, intersection, complement) are valid. Moreover, translation of set I is also defined. For definition of set operations see A.

The morphological operators mainly used are erosion and dilation: they respectively reduce and enlarge the area occupied by foreground pixels.

The dilation of image F is defined as follows:

$$F \oplus I = \left\{(x,y) | I_{(x,y)} \cap F \neq \emptyset\right\} \tag{5}$$

where

$$I = \{(-1,-1),(-1,0),(-1,1),(0,-1),(0,0),(0,1),(1,-1),(1,0),(1,1)\} \tag{6}$$

The erosion of image F is defined as follows:

$$F \ominus I = \left\{(x,y) | I_{(x,y)} \cap F^c \neq \emptyset\right\} \tag{7}$$

Dilation and erosion can be combined together in several ways. In particular they can be used to fill the holes of the image, i.e. to remove background pixels inside foreground objects that result at the end of thresholding, as can be seen in Fig. 3(b): in fact, since in actual masonry mortar areas can not be present inside the stone, these should be removed. This operation, which is described in detail in Appendix A, allows to obtain the image shown in Fig. 3(c).

Thereafter, erosion and dilation operators are applied in succession in order to smooth edges of the stones, obtaining images shown in Fig. 3(d).

3. Statistical analysis of the masonry texture

The aim of the operations described in the present Section is to obtain, starting from the binary image of masonry obtained at the end of preceding Section, the identification of stones and mortar joints and then to perform a statistical analysis which allows to identify the main characteristics of the constituents (size of the stones, dimensions of the joints) and of their spatial relations.

The binary images are analyzed to detect the stones, which are identified with the regions defined using the methods briefly described in Appendix A.

For each stone the following properties can be computed: area A; centroid (x_G, y_G) ; major and minor moments of inertia, J_M and J_m; orientation θ, defined as the angle between the minor principal axis (associated to J_m) and the horizontal axis.

The value of A can be used to remove from the image the stones with $A < \tilde{A}$, where $\tilde{A}$ is a prefixed value, in order to eliminate the stones very small. The result is shown in Fig. 4(a) for the masonry wall #1 and Fig. 4(b) for the masonry wall #2.

Then, the width B and height H of the rectangular equivalent to each stone was found imposing that:

- the area, A, is conserved
- the ratio of moments of inertia, $\frac{J_M}{J_m}$, is conserved.

The values of B and H are therefore given by:

$$H = \left(\frac{A^2}{J_M/J_m}\right)^{1/4} \tag{8a}$$

$$B = \frac{A}{H} \tag{8b}$$

Note that in what follows B always denote the horizontal dimension of the stone while H denote the vertical dimension, while in (8) it was assumed $B \geqslant H$ which corresponds to assume orientation $\theta \in [0, \pi/4]$, therefore if the orientation is greater than $\pi/4$ the value from (8) are switched. Moreover, it is assumed that each rectangle has the same centroid (x_G, y_G) of the stone.

Once the position of the centroid and the dimensions of the stones, assumed to be rectangular, is known it is possible to evaluate the thickness of both bed and head mortar joints. The stone i faces stone j, and therefore a mortar joint is present between the two stones, only if both the following inequalities hold (see Fig. 5):

$$|y_{G,i} - y_{G,j}| \leqslant \frac{H_i}{2} + \frac{H_j}{2} + \Delta_H \tag{9a}$$

$$|x_{G,i} - x_{G,j}| \leqslant \frac{B_i}{2} + \frac{B_j}{2} + \Delta_B \tag{9b}$$

where Δ_B and Δ_H are:

$$\Delta_B = \min\{B_i\} \tag{10a}$$

$$\Delta_H = \min\{H_i\} \tag{10b}$$

To separate head joint from bed joints the following criterion was used. If:

$$|y_{G,i} - y_{G,j}| \leqslant \frac{H_i}{2} + \frac{H_j}{2} \tag{11}$$

than the joint between stones i and j is an head joint, whose thickness and length are given by:

$$t_{ij}^h = |x_{G,i} - x_{G,j}| - \frac{B_i + B_j}{2} \tag{12a}$$

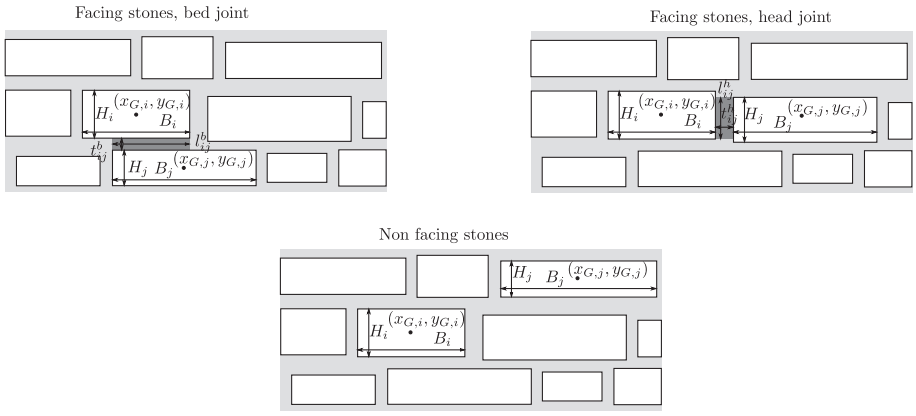

Fig. 5. Identification of facing stones with joint's dimensions.

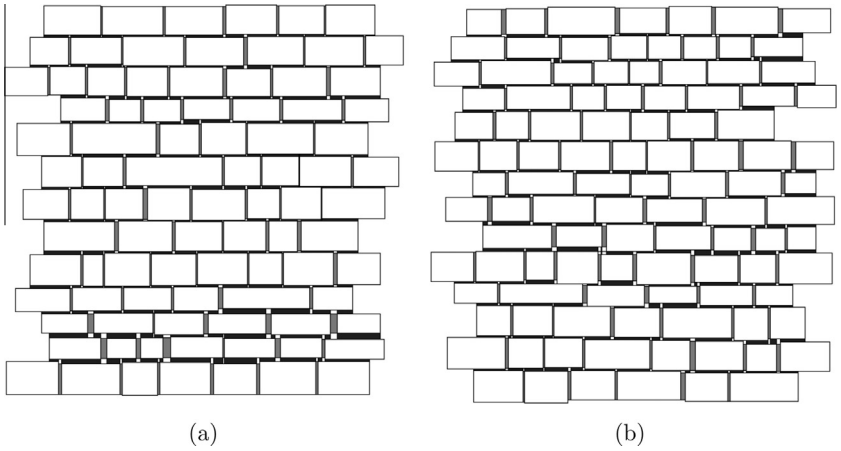

Fig. 6. Image of the wall with equivalent rectangular stones and bed (dark gray) and head (light gray) mortar joint: (a) masonry wall #1, (b) masonry wall #2.

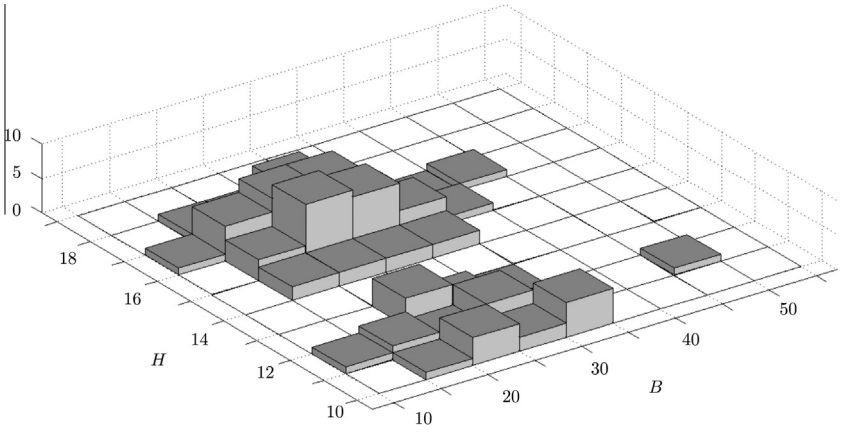

Fig. 7. Joint distribution of B and H for masonry wall #1.

$$l_{ij}^{h} = -\left|y_{G,i} - y_{G,j}\right| + \frac{H_i + H_j}{2} \tag{12b}$$

else the joint between stones i and j is a bed joint, whose thickness is:

$$t_{ij}^{b} = \left|y_{G,i} - y_{G,j}\right| - \frac{H_i + H_j}{2} \tag{13a}$$

$$l_{ij}^{b} = -\left|x_{G,i} - x_{G,j}\right| + \frac{B_i + B_j}{2} \tag{13b}$$

(modification on (12b) and (13b) are necessary when the length of the joint is equal respectively to the height or width of one of the stones)

The proposed approach was applied to the masonry wall #1 (Fig. 1(a)) using binary images shown in Fig. 4(a), obtaining the equivalent rectangular stones and corresponding head and bed joints shown in Fig. 6(a). Note that only entire stones and the corresponding mortar joint between them were used. The equivalent rectangular stones for masonry wall #2 (Fig. 1(b)) using binary image in Fig. 4(b) is shown in Fig. 6(b).

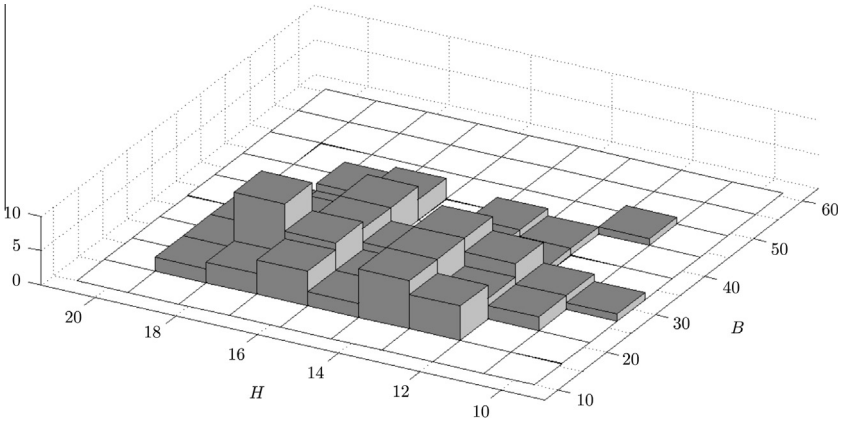

Fig. 8. Joint distribution of B and H for masonry wall #2.

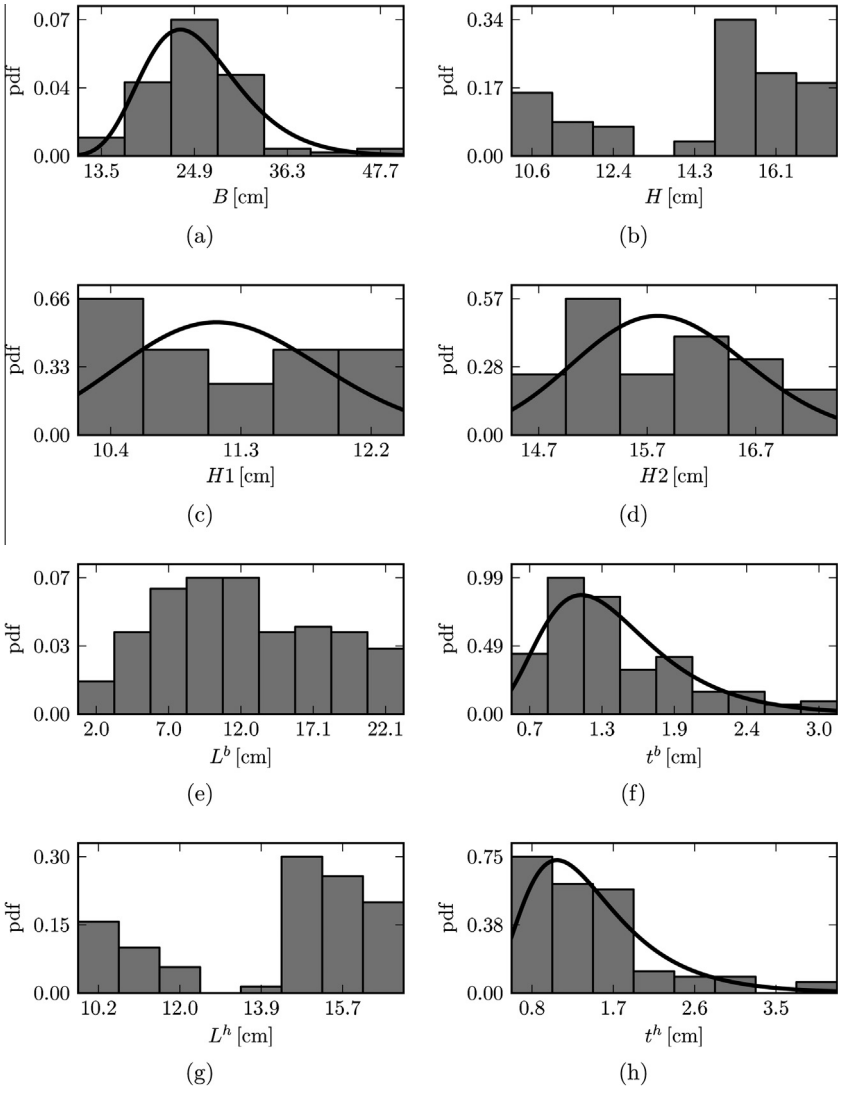

Fig. 9. Estimation of probability density function for masonry wall #1 shown in Fig. 1(a): (a) stones' width, (b) stones' height, (c) height of first family, (d) height of second family, (e) bed joints' length, (f) bed joints' thickness, (g) head joints' length, (h) head joints' thickness.

The joint distribution of dimensions (B and H) of the stones is shown in Fig. 7 for masonry wall #1 and in Fig. 8 for the masonry wall #2. This approach allows to identify possible different families of stones. In the case of masonry wall #1 two families of stones can be identified on the base of their height: one is characterized by an height $H_i \leqslant \tilde{H}$ while the other is characterized by an height $H_i > \tilde{H}$ with $\tilde{H} = 13$ cm; 29% of the stones belongs to the first family, while the remaining 71% belongs to the second family.

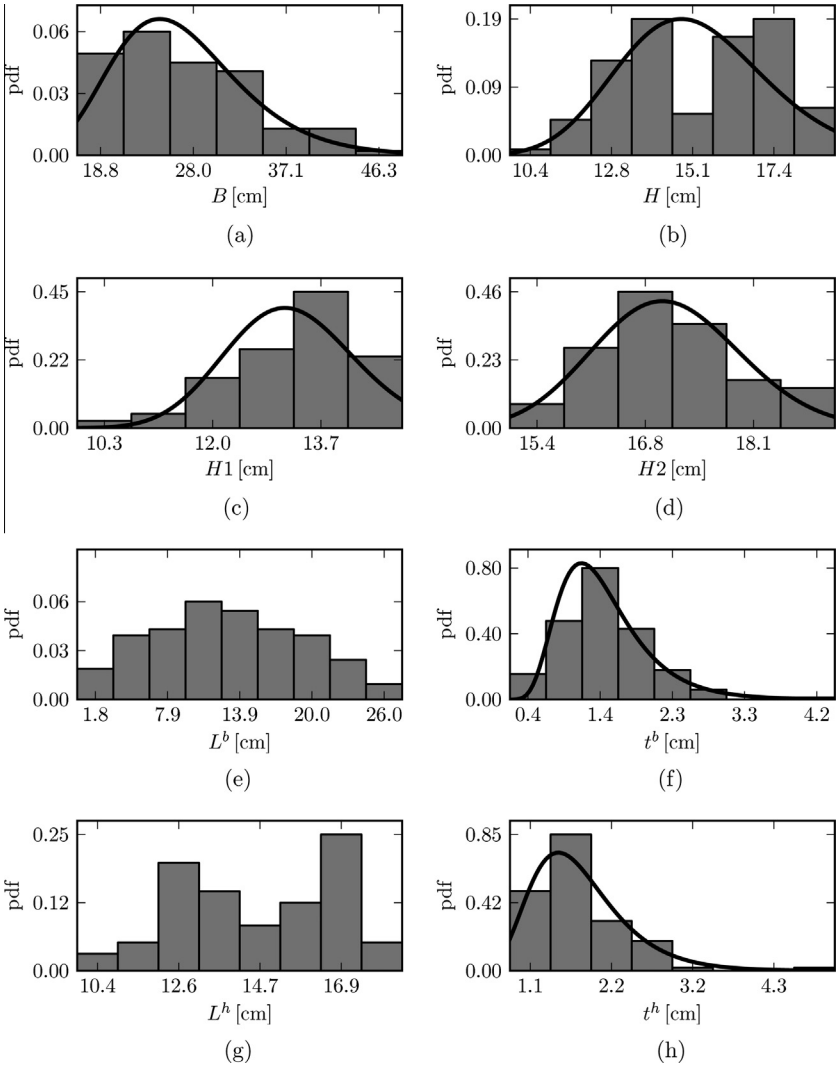

Fig. 10. Estimation of probability density function for masonry wall #2 shown in Fig. 1(b): (a) stones' width, (b) stones' height, (c) height of first family, (d) height of second family, (e) bed joints' length, (f) bed joints' thickness, (g) head joints' length, (h) head joints' thickness.

It is also evident that the distribution of stones width B_i is the same in the two families.

For masonry wall #2 it should be noted that the distribution of the dimensions of the blocks (Fig. 8) shows a slightly grouping in two families but without a definite gap as in the case of masonry #1. From this observation in the parametric description of the periodic cell (in the following Section 4.1) two cases will be considered: a single family of stones and two families with $\tilde{H} = 15$ cm.

Moreover, the probability density function can be estimated for all the relevant geometric characteristics: width and height of the stones, thickness of both head and bed joints. The results are shown in Fig. 9 for the masonry wall #1 and in Fig. 10 for the masonry wall #2. In the figures, for each distribution the curve of log-normal probability density function with same mean and variance is also plotted.

It should be noted that in the case of masonry wall #1 the presence of two families can be assessed, besides what shown in Fig. 9(b), also from the length of head joints (Fig. 9(g)). The apparent increase of the horizontal joints' thickness at the lower part of the wall (Fig. 4(a)) could be superficial and due to imperfections of the geometry of the stones (in practice, masons fill with mortar the missing and broken parts of the stone). This aspect can be resolved by a ad-hoc "fine tuning" operation, or, if it is limited as in the considered masonry, its influence is considered to be negligible by taking into account the whole wall; eventually, to cope with this aspect, different portions of the wall can be considered. In the present study, in order to propose and check a method without intervention of the user, the second approach has been followed.

Moreover, the description of the texture of the wall may be enhanced by another parameter: the coordination number. Its definition is borrowed from crystallography and, for each stone, it is the number of the nearest neighboring stones. Here neighboring stones means that the stones share a mortar joint. The histograms of coordination number is shown in Fig. 11 for both masonries.

It is evident that for both masonry the majority of the stones has coordination number equal to 6.

4. Estimation of the Statistically Equivalent Periodic Unit Cell (SEPUC)

4.1. Parametric description of the periodic cell

The geometrical description of the equivalent periodic cell is strictly based on the choice of the geometrical parameters analyzed in the previous section by means of statistical methods. A

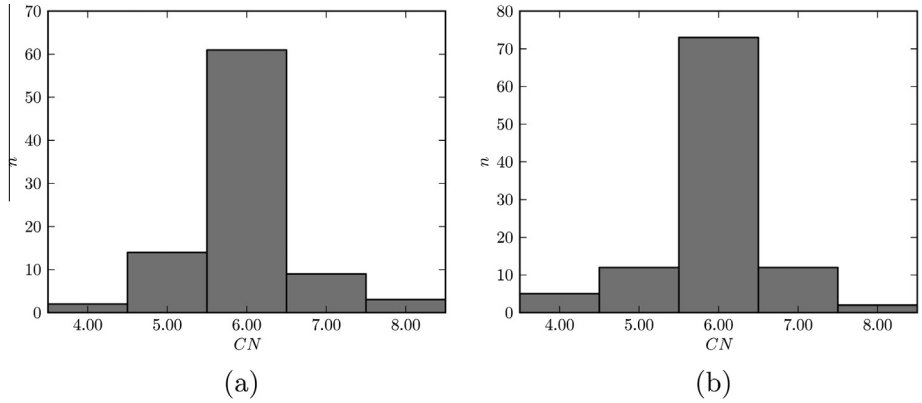

Fig. 11. Coordination number: (a) blocks of masonry wall #1 shown in Fig. 1(a), (b) blocks of masonry wall #2l shown in Fig. 1(b).

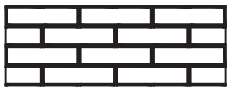

Running bond

$E[B] = D$ (100% $B = D$)

$E[CN] = 6$ (100% $CN = 6$)

$E[l^b] = \frac{1}{2}(D - s)$ (100% $l^b = \frac{1}{2}(D - s)$)

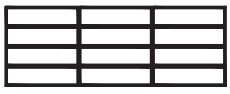

Stack bond

$E[B] = D$ (100% of stones $B = D$)

$E[CN] = 4$ (100% $CN = 4$)

$E[l^b] = D$ (100% $l^b = D$)

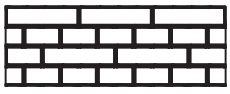

English cross bond

$E[B] = \frac{2}{3}D - \frac{1}{3}t^b$ (33.3% $B = D$ and 66.7% $B = \frac{1}{2}(D - s)$)

$E[CN] = 6$ (33.3% $CN = 8$ and 66.7% $CN = 5$)

$E[l^b] = \frac{1}{3}D - \frac{2}{3}s$ (33.3% $l^b = \frac{1}{2}D - \frac{1}{2}s$ and 66.7% $l^b = \frac{1}{4}D - \frac{3}{4}s$)

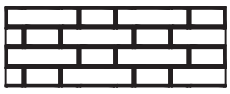

Flemish bond

$E[B] = \frac{3}{4}D - \frac{1}{4}s$ (50% $B = D$ and 50% $\frac{1}{2}(D - s)$)

$E[CN] = 6$ (50% $CN = 8$ and 50% $CN = 4$)

$E[l^b] = \frac{3}{8}D - \frac{7}{16}s$ (50% $l^b = \frac{1}{2}D - \frac{1}{2}s$ and 50% $l^b = \frac{1}{4}D - \frac{3}{8}s$)

Fig. 12. Main characteristics of some periodic masonry textures.

specific number of them must be selected in order to obtain a consistent Statistically Equivalent Texture (SET). These parameters, that represent the minimum number of geometrical descriptors necessary to define the arrangement of the stones and the mortar joints, are accountable for the equivalent texture obtained, by the periodic translation of the cell, and then for its equivalent mechanical response.

In the following, for clearness of explanation, the procedure that leads to the definition of the SET for the masonry wall #1, shown in Fig. 1(a), will be illustrated step-by-step. Nevertheless, a similar procedure was used for the definition of SET for masonry wall #2.

In order to identify the SET, in Fig. 12 some characteristics (width of the stones, coordination number, length of bed mortar joints) for several commonly used periodic textures made by bricks (running bond, stack bond, Flemish bond, English cross bond) are shown. Indicating with D the major dimension of the brick, it is assumed that the other dimensions are $\frac{1}{2}(D - s)$ and $\frac{1}{4}(D - 3s)$, the latter usually being the height, where s is the thickness of mortar joints: for example, the standard "UNI" brick in Italy has $D = 250$ mm (which give dimensions of brick $250 \times 120 \times 55$) and is used with mortar joints having thickness $s = 10$ mm.

Concerning the periodic textures, some considerations which may be helpful in the following can be made. In a running bond texture the length of bed mortar joints is roughly the half of the width of bricks, while in a stack bond pattern it is the very same. The height of the bricks is the same for all the pattern; however, in running and stack bond patterns also the width is the same for all the bricks, while for English and Flemish bond textures the bricks can be separated in two different families relying on the width. The mean value of the coordination number is 6, except for stack bond where it is 4; nevertheless, bricks may have two different coordination numbers (for example, in the English cross bond one third of the bricks have coordination number equal to 8 and two-third of the bricks have coordination number 5).

In the case of masonry wall #1, the Fig. 9(a) highlights that the width of the blocks has a unimodal distribution. Therefore a running or stack bond may be used as reference pattern. Nevertheless, from the Fig. 9(e) a unique mode for the length of the bed joints can be observed, whose value is almost equal to half the mode of blocks width distribution, so that a running bond arrangement for the SET can be taken into account. The choice of a running bond pattern instead of a stack bond is also confirmed by the analysis of coordination number in Fig. 11(a), which indicates a mean value of $CN = 6$ and therefore corresponding to that of the running bond.

It is worth noting that, among all possible arrangements, the running bond texture for masonry with coordination number $CN = 6$ gives an upper bound for the stiffness of the masonry, as shown in Cecchi and Sab (2009).

The evident bimodal distribution of the height of the blocks (Fig. 9(b)) induces to look at the presence of two families of stones,

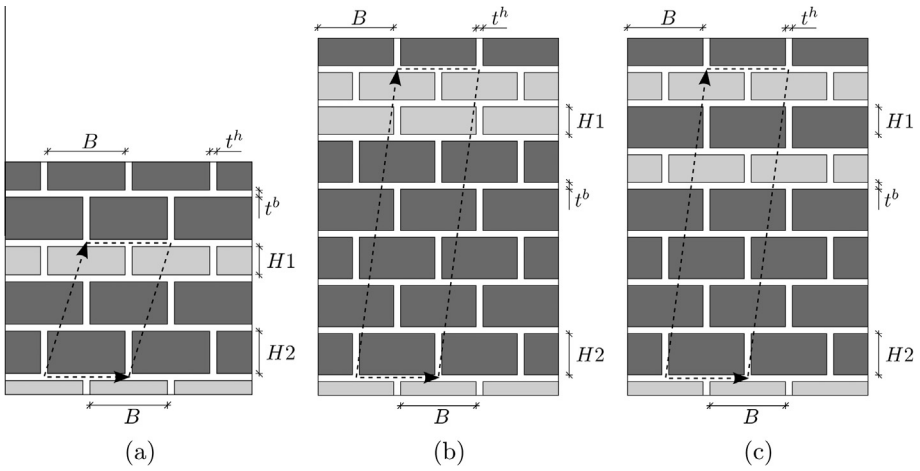

Fig. 13. Statistically Equivalent Textures (SET) for masonry wall #1, obtained by the periodic translation of the cell with (a) three and (b) and (c) seven rows.

relying on the values of height ($H1$ the minor and $H2$ the greater). Therefore the actual texture of the wall, with stones laid out in rows of constant height, can be considered to be quasi-periodic according to the definition given in the Introduction. This feature can also be directly attained by the comparison between the probability distributions of the heights of the blocks and of the lengths of the head joints (Fig. 9(b) and (g)), that show almost the same probability density.

In the masonry wall the ratio between the number of stones with height $H2$ and $H1$ is about 2.4. For this reason three types of texture have been studied (Fig. 13): the first contains the periodic repetition of three rows, with ratio 2:1 between the height values, and the others are characterized by seven rows, with a ratio of 5:2. In the first case there is only a possible sequence of row heights [$H2$-$H2$-$H1$]. In the second case two sequences have been considered, [$H2$-$H2$-$H2$-$H2$-$H2$-$H1$-$H1$] and [$H2$-$H2$-$H2$-$H2$-$H1$-$H2$-$H1$]. In this way the fundamental parameters able to fully describe the equivalent texture are the width B, the heights $H1$ and $H2$, and the thickness of bed and head joints, t^b and t^h respectively. The three textures considered are shown in Fig. 13, while the three periodic cell together with the corresponding translation vector base which allows to generate the wall texture are shown in Fig. 14.

In the case of masonry wall #2, the same arguments used for masonry wall #1 permit to assume a SET with a running bond pattern. Moreover, following the analysis of stone heights (Section 3) two different types of textures have been studied: the first one is made of a single family of stones, and therefore is indicated with [H], while the second is made by the repetition of two rows with stones of height $H1$ and $H2$ with a ratio 1:1 and therefore with sequence [$H2$-$H1$]; the two textures are shown in Fig. 15.

The two cells represented in Fig. 16 have been chosen for the proposed textures. It is worth noting that the choice of the cell in Fig. 16(b), which is not the smallest possible, was dictated by the necessity to use the same periodic boundary conditions assumed for masonry wall #1 and discussed in Section 5.1.

Maybe it is not surprising that in both cases the SET consists in a running bond pattern. When the mason builds a masonry using stones of different dimensions, the state-of-the-art laws suggest that each row have stones of about the same height. Moreover, they also impose that vertical (head) joints should not be aligned, and the mason will try to place the head joint approximately near the middle of the beneath stone. Therefore, although the random width of the stones, the arrangement of the head joints tends to be that of a running bond pattern, given that the stack bond is structural weaker than the others and that the English cross or

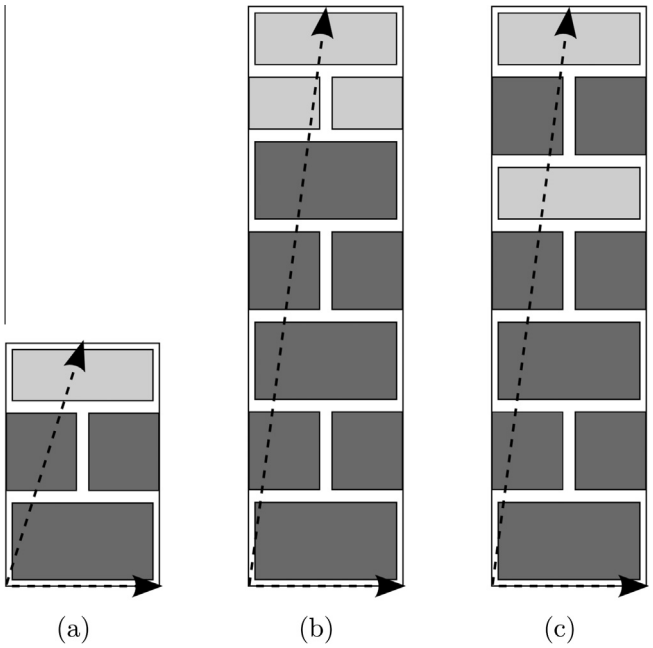

Fig. 14. Periodic cells analyzed for the characterization of the textures used for masonry wall #1 and shown in Fig. 13.

Flemish bond textures require the availability of two well distinct groups of stones, each with almost the same width. This latter requirement could be difficult to fulfill in the case of stones not artificially made (bricks). This is not the case of the masonries considered in the present study where the width of the stones is described by a single probabilistic density law with one mode. Nevertheless the proposed method, based on a probabilistic regularization of quasi periodic patterns, appears to be easily applicable to geometric characteristics with bimodal densities adopting the same approach used for the height of the stones in masonry #2 (analysis with different patterns and comparison).

4.2. Generation of periodic unit cell samples

What follows is valid for the SET of masonry wall #1 (shown in Fig. 1(a)). Nevertheless similar operations are valid for the SET of masonry wall #2 (shown in Fig. 1(b)). The generation of periodic

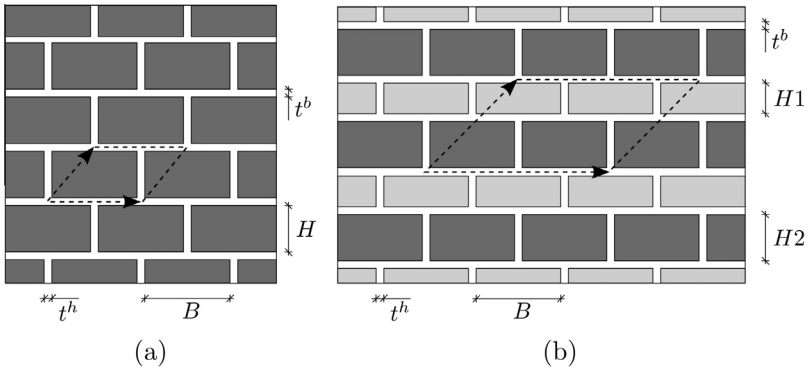

Fig. 15. Statistically Equivalent Textures (SET) for masonry wall #2, obtained by the periodic translation of the cell with (a) a single family and (b) two families of stones.

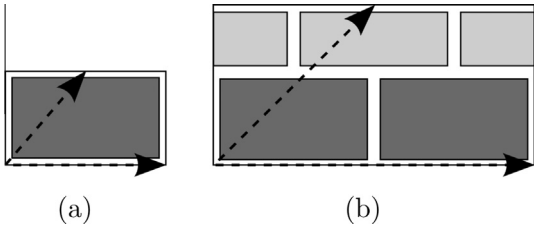

Fig. 16. Periodic cells analyzed for the characterization of the textures used for masonry wall #2 and shown in Fig. 15.

Table 1
Parameters of log-normal distributions for generated quantities of masonry wall #1.

x	$\bar{x}$	s^2	μ	σ^2
B	25.418	40.991	3.205	0.062
$H1$	11.202	0.559	2.414	0.004
$H2$	15.865	0.666	2.763	0.003
t^b	1.397	0.311	0.262	0.148
t^h	1.485	0.498	0.294	0.204

unit cell was achieved by taking into account the following geometrical characteristics discussed in the previous section:

- height of stones of the first family, $H1$;
- height of stones of the second family, $H2$;
- width of stones, B, valid for both families;
- thickness of bed mortar joints, t^b;
- thickness of head mortar joints, t^h;

The mean value, $\bar{x}$, and the variance, s^2, of each geometrical characteristic shown in Fig. 9 have been evaluated. Moreover, the parameters μ and σ^2 of the log-normal distribution of each quantity, which correspond to the mean and standard deviation of the underlying normal distribution, are reported together with the preceding values in Table 1. The values of μ and σ^2 have been used to generate the samples.

It was assumed independence between t^b, t^h and the other quantities. Nevertheless, statistical analysis suggests a correlation between width B_i and height H_i for both families, that can be expressed as:

$$R = \begin{bmatrix} 1 & \rho_1 & \rho_2 \\ \rho_1 & 1 & 0 \\ \rho_2 & 0 & 1 \end{bmatrix} = \begin{bmatrix} 1 & -0.14 & -0.18 \\ -0.14 & 1 & 0 \\ -0.18 & 0 & 1 \end{bmatrix} \tag{14}$$

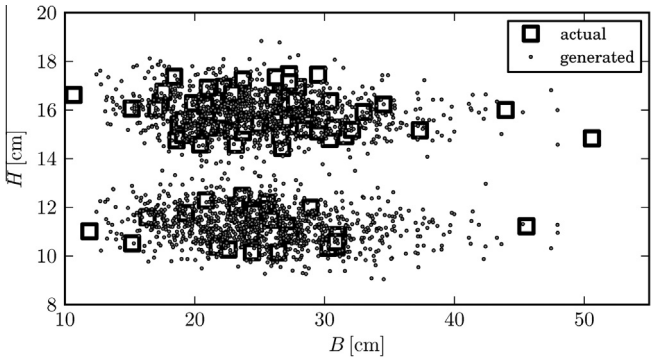

Fig. 17. Actual and generated values of B and H for masonry wall #1.

where:

$$\rho_i = \frac{\mathrm{E}_i[(B - \mathrm{E}_i[B]) \cdot (H - \mathrm{E}_i[H])]}{\sqrt{\mathrm{E}_i\left[(B - \mathrm{E}_i[B])^2\right] \cdot \mathrm{E}_i\left[(H - \mathrm{E}_i[H])^2\right]}} \tag{15}$$

where $\mathrm{E}_i[\cdot]$ denote the average operator $\mathrm{E}[\cdot]$ evaluated taking into account only stones of the family with height Hi.

The logarithm of generated values of $B, H1$ and $H2$, indicated as $\widehat{B}, \widehat{H1}$ and $\widehat{H2}$, were placed into column vectors $\underline{\widehat{B}}, \underline{\widehat{H1}}, \underline{\widehat{H2}}$. The values in these vectors, scaled to have zero mean and unit variance, are placed in the matrix:

$$G = \left[\underline{\widehat{B}}, \underline{\widehat{H1}}, \underline{\widehat{H2}}\right] \tag{16}$$

Eventually, the correlation expressed by R can be obtained multiplying G by $\sqrt{\widehat{R}}$ (Miller and Childers, 2004) where:

$$\widehat{R} = \begin{bmatrix} 1 & \hat{\rho}_1 & \hat{\rho}_2 \\ \hat{\rho}_1 & 1 & 0 \\ \hat{\rho}_2 & 0 & 1 \end{bmatrix} \tag{17}$$

and $\hat{\rho}_i$ are evaluated similarly to ρ_i with (15) using $\widehat{B}, \widehat{H1}$ and $\widehat{H2}$ instead of $B, H1$ and $H2$.

After re-scaling, the values of $B, H1$ and $H2$ with the desired values of mean, variance and correlation coefficients are obtained.

A total of 1000 samples were generated. The results for B and H are shown in Fig. 17 .

In the case of masonry wall #2 the mean $\bar{x}$ and variance s^2 estimated from statistical analysis, as shown in Fig. 10, and the parameters μ and σ^2 of the associated log-normal distribution are reported in Table 2 for each quantity of interest.

Also in this case total of 1000 samples were generated. The results for B and H are shown in Fig. 18.

Table 2
Parameters of log-normal distributions for generated quantities of masonry wall #2.

x	$\bar{x}$	s^2	μ	σ^2
B	26.918	44.010	3.264	0.058
H	15.212	4.644	2.712	0.021
$H1$	13.217	1.036	2.578	0.006
$H2$	17.059	0.885	2.835	0.003
t^b	1.414	0.344	0.251	0.222
t^h	1.775	0.394	0.519	0.105

Both for masonry wall #1 and masonry wall #2, Figs. 17 and 18 show a good agreement between generated and actual values of stones dimensions and of their correlation.

4.3. Identification of SEPUC

The Statistically Equivalent Periodic Unit Cell is defined as a cell that, when arranged in the periodic pattern according to SET, originates a texture which, globally, is equivalent to the actual masonry. The criterion which permits to consider the equivalence effective is based on the minimization of an error function $\mathcal{F}(\Omega_i)$, where Ω_i with $i = 1, 2, \ldots, 1000$ is the ith sample. The definition of $\mathcal{F}(\Omega_i)$ use n geometrical parameters $\mathcal{X}_{k,i}$ (dimensions of the blocks and of the mortar joints) and the concentration ratio $c_{1,i}$, defined as the percentage of the area of masonry wall occupied by the blocks, of each sample as follows:

$$\mathcal{F}(\Omega_i) = \frac{1}{n+1}\left(\sum_{k=1}^{n}\frac{|\,\mathcal{X}_{k,i} - \bar{\mathcal{X}}_k\,|}{\bar{\mathcal{X}}_k} + \frac{|\,c_{1,i} - \check{c}_1\,|}{\check{c}_1}\right) \tag{18}$$

where $\bar{\mathcal{X}}_k$ is the mean of geometrical parameter $\mathcal{X}_k$ and $\check{c}_1$ is the concentration ratio of the entire wall. In the case of masonry wall #1, for all types of SET (Fig. 14) $n = 5$, and $\mathcal{X}_1 = B, \mathcal{X}_2 = H1, \mathcal{X}_3 = H2, \mathcal{X}_4 = t^b$ and $\mathcal{X}_5 = t^h$, while in the case of masonry wall #2, for first type of SET (Fig. 16(a)) $n = 4$, and $\mathcal{X}_1 = B, \mathcal{X}_2 = H, \mathcal{X}_4 = i^b$ and $\mathcal{X}_5 = t^h$ and for second type of SET (Fig. 16(b)) $n = 5$, and $\mathcal{X}_1 = i, \mathcal{X}_2 = H1, \mathcal{X}_3 = H2, \mathcal{X}_4 = t^b$ and $\mathcal{X}_5 = t^h$.

The choice of the error function (18) has been made according to the following considerations:

- the existence of a correlation between the concentration ratio of the strong phase and the stiffness of the masonry requires to minimize the difference between $c_{1,i}$ and $\check{c}_1$;
- the minimization of the previous difference may lead to dimensions of blocks and joints not representative of the actual ones and so the minimization of the difference from the mean values of geometrical parameters is required.

Nevertheless, in order to assess the influence of each of the preceding factors, and to evaluate the effect of considering a different statistics (median instead of the mean), four other criteria have been considered:

- $\mathcal{F}^*_A(\Omega_i) = \frac{1}{n}\sum_{k=1}^{n}\frac{|\mathcal{X}_{k,i} - \tilde{\mathcal{X}}_k|}{\tilde{\mathcal{X}}_k}$
- $\mathcal{F}^*_B(\Omega_i) = \frac{1}{n}\sum_{k=1}^{n}\frac{|\mathcal{X}_{k,i} - \tilde{\mathcal{X}}_k|}{\tilde{\mathcal{X}}_k}$
- $\mathcal{F}^*_C(\Omega_i) = \frac{|c_{1,i} - \check{c}_1|}{\check{c}_1}$
- $\mathcal{F}^*_D(\Omega_i) = \frac{1}{n+1}\left(\sum_{k=1}^{n}\frac{|\mathcal{X}_{k,i} - \tilde{\mathcal{X}}_k|}{\tilde{\mathcal{X}}_k} + \frac{|c_{1,i} - \check{c}_1|}{\check{c}_1}\right)$

where $\tilde{\mathcal{X}}_k$ is the median of $\mathcal{X}_k$.

5. Numerical analysis

5.1. Definition of the periodic boundary conditions

The definition of a periodic cell implies the explanation of the periodic boundary conditions which assure the periodicity of the deformations and the anti-periodicity of the stresses (Anthoine, 1995). These conditions depend not only on the geometry of the cell but also on its translation vector base. The cells of Fig. 14 are characterized by six nodes that identify six boundary portions on which the periodicity conditions are defined (Fig. 19). Only three of the six nodes are representative of the translation vector base, in this case the nodes 1, 2 and 6, that are generally called "controlling points".

Following the mathematical approach of Mistler et al. (2007), the generic states of macroscopic stress and strain of the cell, expressed through tensors $\langle\boldsymbol{\sigma}\rangle$ and $\langle\boldsymbol{\varepsilon}\rangle$ respectively, can be obtained by the definition of specific conditions in terms of forces and/or

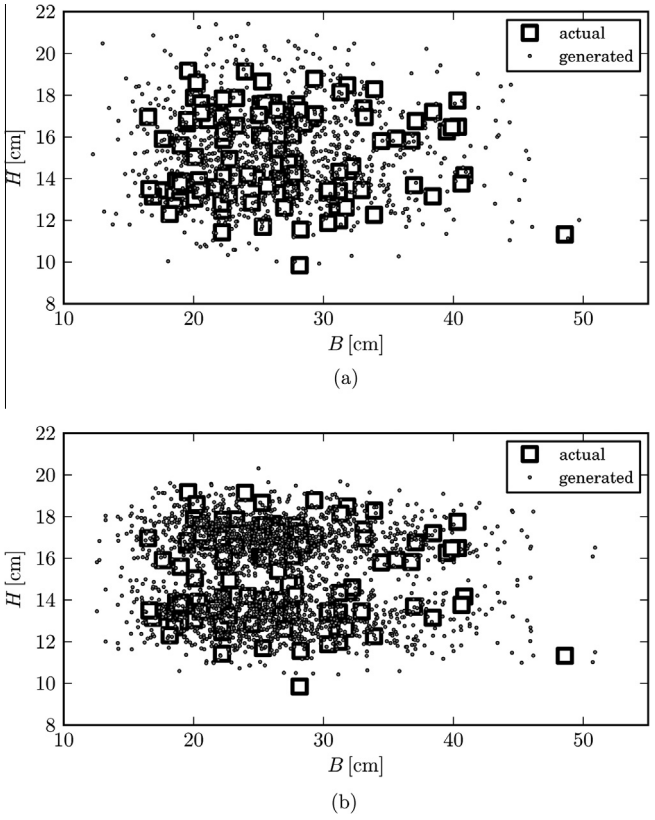

Fig. 18. Actual and generated values of B and H for masonry wall #2: (a) one family of stone heights, (b) two families of stone heights.

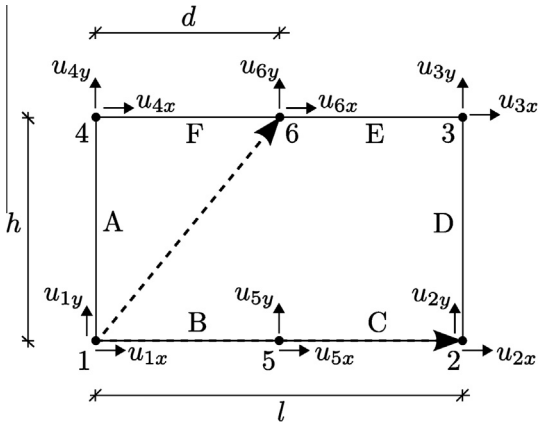

Fig. 19. Translation system and periodic reference system of the cell.

displacements on three of the six degree of freedom of the controlling points, u_{2x}, u_{2y} and u_{6y}, called master d.o.f. The other d.o.f. of the controlling points are restrained or constrained in order to inhibit any rigid translation and rotation of the cell:

$$\begin{cases} u_{1x} = u_{1y} = 0 \\ u_{6x} = \frac{d}{l} u_{2x} + \frac{h}{l} u_{2y} \end{cases} \tag{19}$$

in which l, h and d are the geometric parameters describing the dimensions of the cell and of the periodic translation vector base (Fig. 19). The relation $l = 2d$ can be easily derived. The periodicity conditions in vector format are:

$$\mathbf{u}_D - \mathbf{u}_A = \mathbf{u}_2 - \mathbf{u}_1 \tag{20a}$$

$$\mathbf{u}_E - \mathbf{u}_B = \mathbf{u}_6 - \mathbf{u}_1 \tag{20b}$$

$$\mathbf{u}_F - \mathbf{u}_C = \mathbf{u}_6 - \mathbf{u}_2 \tag{20c}$$

which,expanding each component and taking into account the boundary conditions (19), become:

$$u_{Dx} - u_{Ax} - u_{2x} = 0 \tag{21a}$$

$$u_{Dy} - u_{Ay} - u_{2y} = 0 \tag{21b}$$

$$u_{Ex} - u_{Bx} - \frac{1}{2} u_{2x} + \frac{h}{l} u_{2y} = 0 \tag{21c}$$

$$u_{Ey} - u_{By} - u_{6y} = 0 \tag{21d}$$

$$u_{Fx} - u_{Cx} - \frac{1}{2} u_{2x} + \frac{h}{l} u_{2y} = 0 \tag{21e}$$

$$u_{Fy} - u_{Cy} - u_{6y} + u_{2y} = 0 \tag{21f}$$

Specific values of boundary conditions to be assigned at the master nodes determine predefined macroscopic tension $\langle \boldsymbol{\sigma} \rangle$ or strain $\langle \boldsymbol{\varepsilon} \rangle$ tensors over the cell, so that the effective macroscopic stiffness elastic tensor $\mathbf{C}$ can be directly obtained through the relation:

$$\langle \boldsymbol{\sigma} \rangle = \langle \mathbf{C} : \boldsymbol{\varepsilon} \rangle \tag{22}$$

Considering the following three elementary tensors:

$$\mathbf{I}^{11} = \begin{bmatrix} 1 & 0 \\ 0 & 0 \end{bmatrix}, \quad \mathbf{I}^{22} = \begin{bmatrix} 0 & 0 \\ 0 & 1 \end{bmatrix}, \quad \mathbf{I}^{12} = \mathbf{I}^{21} = \begin{bmatrix} 0 & 1 \\ 1 & 0 \end{bmatrix} \tag{23}$$

the components of tensor $\mathbf{C}$ are obtained by means of a strain approach, i.e. by analyzing the three cases $\langle \boldsymbol{\varepsilon} \rangle = \mathbf{I}^{ij}$ through the relations:

$$u_{2x} = l \langle \varepsilon_{11} \rangle \tag{24a}$$

$$u_{2y} = l \langle \varepsilon_{22} \rangle \tag{24b}$$

$$u_{6y} = h \langle \varepsilon_{22} \rangle + l \langle \varepsilon_{12} \rangle \tag{24c}$$

5.2. Results and discussion

The periodic cells generated as described in Section 4.2 have been analyzed with the periodic boundary conditions described in the Section 5.1 by means of the finite element method. For each cell the elastic stiffness tensor has been estimated. The analyses have been performed in the elastic field using 4-node elements (Cavalagli et al., 2011). For both masonry walls, the elastic characteristics assigned to the blocks (E_b, ν_b) and mortar (E_m, ν_m) are the same used in Cavalagli et al. (2011), i.e. $E_b = 6740$ MPa, $\nu_b = 0.167$, $E_m = 1700$ MPa and $\nu_m = 0.2$. This have permitted to validate the proposed criterion by comparing the results in terms of effective elastic properties of the homogenized continuum. In Fig. 20 the stress fields for a generic statistically periodic cell for each texture of masonry wall #1 are shown for each case of boundary conditions applied, in particular the stress component σ_{11} is represented for the case $\langle \boldsymbol{\varepsilon} \rangle = \mathbf{I}^{11}$, σ_{22} for $\langle \boldsymbol{\varepsilon} \rangle = \mathbf{I}^{22}$ and σ_{12} for $\langle \boldsymbol{\varepsilon} \rangle = \mathbf{I}^{12}$.

The Frobenius norm of the stiffness matrices calculated for each generated cells, together with the limits of Reuss and Voigt, are plotted versus c_1 in Fig. 21 for masonry wall #1 and in Fig. 24 for masonry wall #2. In the same Figures, the points corresponding to the samples which minimize criteria $\mathcal{F}, \mathcal{F}_A^*, \mathcal{F}_B^*, \mathcal{F}_C^*$ and $\mathcal{F}_D^*$ are highlighted. For masonry wall #1 the results concerning the texture [*H2-H2-H2-H2-H1-H2-H1*] are not shown because they are very similar to those of texture [*H2-H2-H2-H2-H2-H1-H1*], with differences of less than 1 ‰.

The analysis of Fig. 21(a) and (b) and Fig. 24(a) and (b) highlights that, in terms of the effective elastic properties, the behavior of the textures is quite similar. Therefore, in order to reduce the computational burden, is more convenient to use the texture with three rows of stone, [*H2-H2-H1*], in the case of masonry wall #1, and with a single family of stones, [*H*], in the case of masonry wall

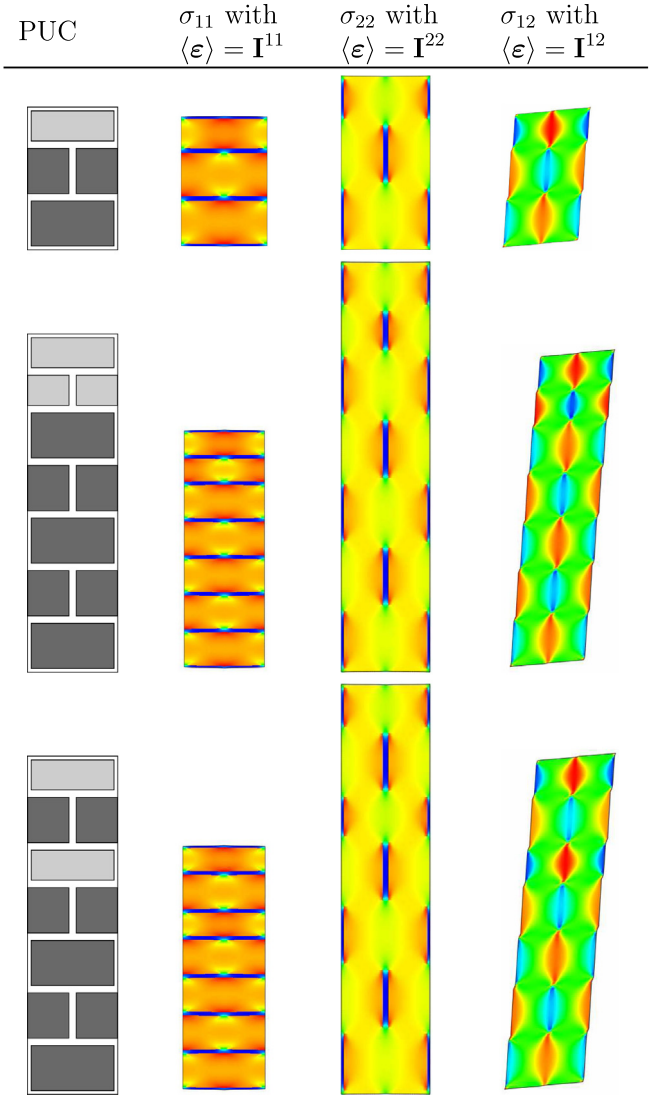

Fig. 20. Stress fields for the generic periodic unit cell of masonry wall #1 for different boundary conditions applied.

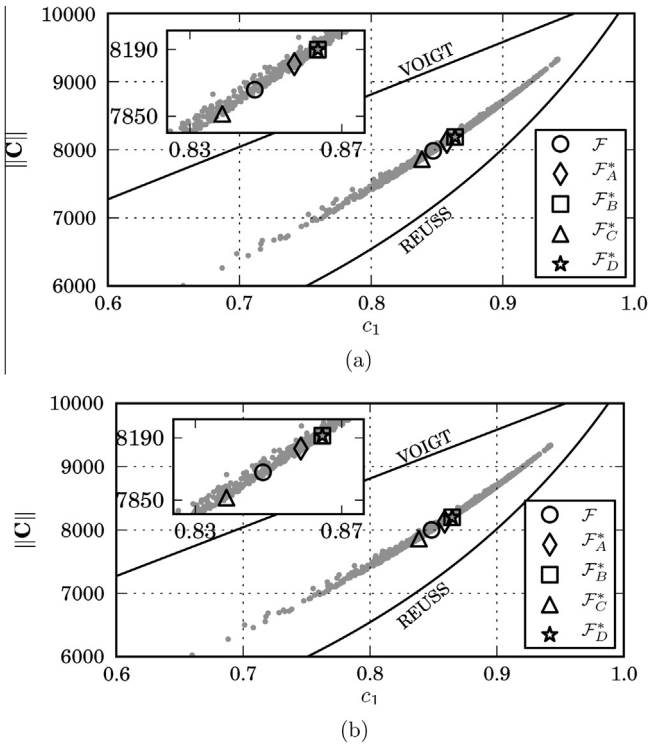

Fig. 21. Frobenius norm of the elastic stiffness tensor for the generated samples of periodic unit cell for masonry wall #1: (a) texture [*H2-H2-H1*] (Fig. 14(a)), (b) texture [*H2-H2-H2-H2-H2-H1-H1*] (Fig. 14(b)).

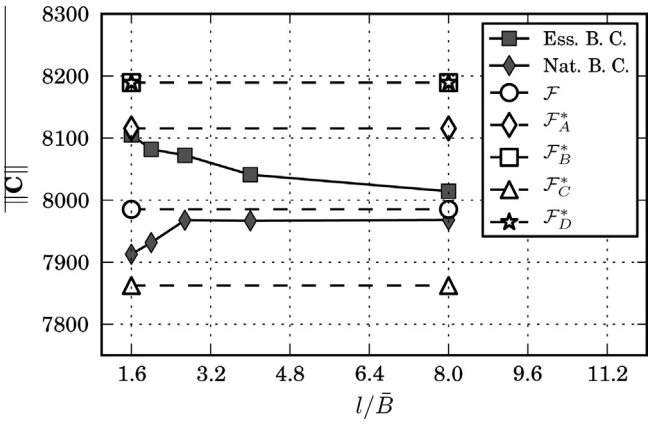

Fig. 22. Comparison of results obtained for masonry wall #1 using SEPUC and those obtained using the "test-windows" method with essential and natural boundary conditions.

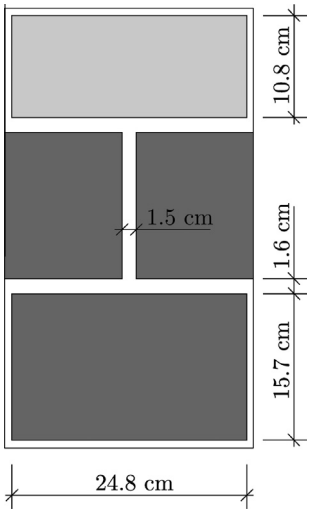

Fig. 23. Statistically Equivalent Periodic Unit Cell for masonry wall #1.

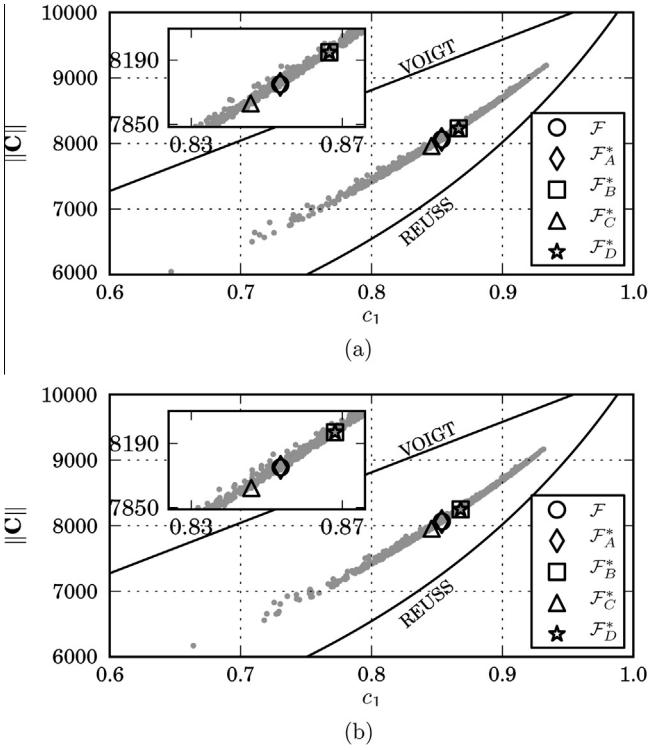

Fig. 24. Frobenius norm of the elastic stiffness tensor for the generated samples of periodic unit cell for masonry wall #2: (a) single family texture (Fig. 16(a)), (b) texture [*H2-H1*] (Fig. 16(b)).

#2. Moreover the figures also show the correlation between concentration ratio of the strong phase and the stiffness of the masonry recalled in Section 4.3.

Within this textures, the criteria introduced in Section 4.3 pick out five SEPUCs, one for each error function ($\mathcal{F}, \mathcal{F}_A^*, \mathcal{F}_B^*, \mathcal{F}_C^*, \mathcal{F}_D^*$): two of the SEPUCs, those associated with $\mathcal{F}_B^*$ and $\mathcal{F}_D^*$, are the same in the case of masonry wall #1 (Fig. 21); two pairs, those associated with $\mathcal{F}$ and $\mathcal{F}_A^*$ and with $\mathcal{F}_B^*$ and $\mathcal{F}_D^*$, are the same in the case of masonry wall #2 (Fig. 24). It should be noted that the concentration ratio is correlated with the stones' dimensions and the joints' thickness. Nevertheless this relationship can be assumed deterministic only in the case of periodic masonry, whereas when dealing with quasi periodic masonry the relationship between the mean (or median) of the geometric characteristics and the concentration ratio of the wall is probabilistic. For this reason the concentration ratio has been considered to be unrelated to the stones' dimensions and the joints' thickness in the criteria $\mathcal{F}$ (Eq. (18)) and with a weight equal to those of each geometric characteristics. In general, the criteria which minimize the difference in terms of geometric parameters and the criterion relative to concentration ratio only assume minimum values at two different generated samples, none of which is the sample which minimize the proposed criterion $\mathcal{F}$ (Eq. (18)). The occasional coincidence of the SEPUC for two different criteria may be due to the inherent characteristics of the original masonry (for example masonry wall #2

Table 3
Geometrical parameters and Frobenius of the elastic stiffness tensor of masonry wall #1 for the SEPUC according to each criterion (values in cm and MPa).

SEPUC	Crit.	B	$H1$	$H2$	t^h	t^b	$\|\mathbf{C}\|$
[$H2$-$H2$-$H1$]	$\mathcal{F}$	24.8	10.8	15.7	1.6	1.5	7985.1
	$\mathcal{F}^*_A$	24.3	11.0	16.0	1.5	1.4	8115.5
	$\mathcal{F}^*_B$	23.1	11.6	16.0	1.3	1.4	8189.4
	$\mathcal{F}^*_C$	15.7	10.8	15.5	1.2	1.6	7862.5
	$\mathcal{F}^*_D$	23.1	11.6	16.0	1.3	1.4	8189.4
[$H2$-$H2$-$H2$-$H2$-$H2$-$H1$-$H1$]	$\mathcal{F}$	24.8	10.8	15.7	1.6	1.5	8001.7
	$\mathcal{F}^*_A$	24.3	11.0	16.0	1.5	1.4	8131.6
	$\mathcal{F}^*_B$	23.1	11.6	16.0	1.3	1.4	8202.1
	$\mathcal{F}^*_C$	19.1	10.8	16.2	1.6	1.4	7863.2
	$\mathcal{F}^*_D$	23.1	11.6	16.0	1.3	1.4	8202.1

Table 4
Components of the elastic stiffness tensor of masonry wall #1 evaluated with "test-windows" method in essential and natural boundary conditions for $l/\bar{B} = 8.0$ and with periodic boundary conditions on SEPUC (values in MPa).

ij	Ess. B.C.	Nat. B.C.	SEPUC
11	5590.0	5554.6	5581.5
12	1006.9	1006.0	855.8
22	5194.6	5168.8	5208.6
33	1991.8	1972.7	2003.5

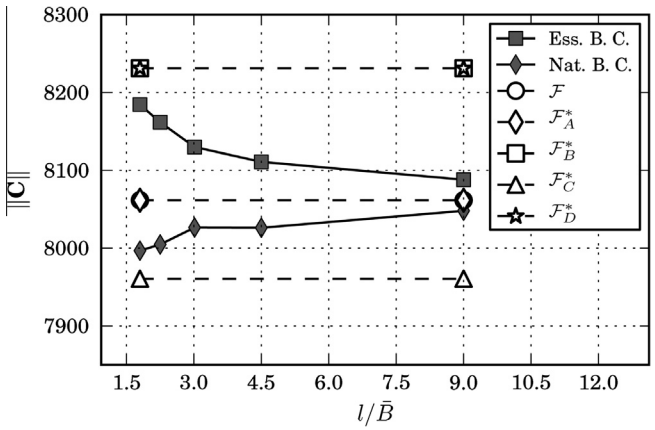

Fig. 25. Comparison of results obtained for masonry wall #2 using SEPUC and those obtained using the "test-windows" method with essential and natural boundary conditions.

seems more regular than masonry wall #1) and to the peculiar outcomes of the Monte Carlo simulations with a limited number of samples. Comparing the results with those obtained by the classical homogenization approaches (Cavalagli et al., 2011), shown in Fig. 22 and in Table 3 for masonry wall #1 and in Fig. 25 and in

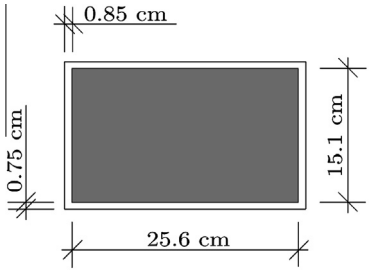

Fig. 26. Statistically Equivalent Periodic Unit Cell for masonry wall #2.

Table 6
Components of the elastic stiffness tensor of masonry wall #2 evaluated with "test-windows" method in essential and natural boundary conditions for $l/\bar{B} = 9.0$ and with periodic boundary conditions on SEPUC (values in MPa).

ij	Ess. B.C.	Nat. B.C.	SEPUC
11	5601.1	5569.9	5572.3
12	1021.4	1021.2	869.2
22	5279.6	5257.3	5316.8
33	2020.4	2004.0	2039.3

Table 5 for masonry wall #2, the proposed criterion $\mathcal{F}(\Omega_i)$, defined by (18), which minimize both the difference from the mean values of geometrical parameters and from the actual concentration ratio, appears the best to identify a periodic cell able to represent the elastic response of the entire wall. It is also shown in Table 3 and Table 5 that the minimization of difference of the concentration ratio alone, $\mathcal{F}^*_C(\Omega_i)$, leads to a cell with dimensions of stones and mortar joints quite different from the mean values of actual texture, as anticipated in Section 4.3. The converse is also true: even if the Monte Carlo generation should generate a sample with exactly the mean of the parameters $\mathcal{X}_k$, which is unlikely, this would have a concentration ratio different from the actual one, and so $\mathcal{F}$

Table 5
Geometrical parameters and Frobenius of the elastic stiffness tensor of masonry wall #2 for the SEPUC according to each criterion (values in cm and MPa).

SEPUC	Crit.	B	H		t^h	t^b	$\|\mathbf{C}\|$
[H]	$\mathcal{F}$	25.6	15.1		1.7	1.5	8061.5
	$\mathcal{F}^*_A$	25.6	15.1		1.7	1.5	8061.5
	$\mathcal{F}^*_B$	26.4	15.2		1.7	1.3	8231.2
	$\mathcal{F}^*_C$	26.4	17.8		2.3	1.5	7960.5
	$\mathcal{F}^*_D$	26.4	15.2		1.7	1.3	8231.2
	Crit.	B	$H1$	$H2$	t^h	t^b	$\|\mathbf{C}\|$
[$H2$-$H1$]	$\mathcal{F}$	25.6	13.2	17.0	1.7	1.5	8062.9
	$\mathcal{F}^*_A$	25.6	13.2	17.0	1.7	1.5	8062.9
	$\mathcal{F}^*_B$	26.0	13.3	18.2	1.7	1.3	8249.0
	$\mathcal{F}^*_C$	19.9	13.4	18.6	1.7	1.4	7954.1
	$\mathcal{F}^*_D$	26.0	13.3	18.2	1.7	1.3	8249.0

could not be null. The SEPUCs that satisfy the proposed criterion for masonry #1 and masonry wall #2 are shown in Fig. 23 and in Fig. 26 respectively and the components of the elastic stiffness tensor compared with those obtained by the classical homogenization approaches are shown in Table 4 and in Table 6.

6. Conclusions

The structural analysis of historical masonry constructions often presents as a crucial task, due to the non-periodicity texture, the definition of the mechanical characteristics of the homogenized continuum. In this paper a method for the estimation of a Statistically Equivalent Periodic Unit Cell (SEPUC) corresponding to a masonry with quasi-periodic texture is proposed. The SEPUC can subsequently be used for the estimation of mechanical characteristics of the masonry with one of the well established methods proposed in literature for periodic media. The aim is to provide a suitable and easy-to-use tool to the engineer.

Starting from a digital image of a masonry wall, the procedure lead to the definition of a SEPUC by means of Digital image processing techniques and of statistical analysis of the constituents geometrical parameters. In particular, after a consistent separation of the phases, the geometrical parameters of the stones and of the mortar joints are analyzed. This allows to identify the characteristics of the actual texture of the masonry, which are used to generate several periodic unit cell, candidate to be the SEPUC. The cells are then analyzed with a finite element model, with the application of periodic boundary conditions, in order to obtain the equivalent elastic stiffness tensor. The choice of SEPUC is made with a proposed criterion which take into account both the dimensions of the stones and mortar joints and the concentration ratio of the phases. It is worth noting that the elastic analysis is used as a suitable tool to validate the reliability of the identification of the SEPUC among all possibilities. In fact the proposed criterion gives the best results when compared with the effective elastic properties obtained by classic homogenization techniques.

As a development of the research, the SEPUC will allow to analyze the non-linear behavior of the masonry by a multi-scale approach.

Acknowledgments

The authors wish to thank the Reviewers for their careful and insightful comments which permitted to enhance the quality of the paper. This research was partially supported by Regione Umbria, within ESF-funded research-grant Scheme.

Appendix A. Morphological operations using set definition for images

A.1. Set operations

If Q and S are two set that represent two input images, the usual set operations can be used to obtain a third set P which represents the output image:

$$P = Q \cup S \Rightarrow P = \{(x,y)|(x,y) \in Q \text{ or } (x,y) \in S\} \tag{A.1}$$

$$P = Q \cap S \Rightarrow P = \{(x,y)|(x,y) \in Q \text{ and } (x,y) \in S\} \tag{A.2}$$

$$P = Q^c \Rightarrow P = \{(x,y)|(x,y) \notin Q\} \tag{A.3}$$

Moreover translation is defined as:

$$P = Q_{(x,y)} \Rightarrow P = \{(s,t)|(s,t) = (a+x, b+y) \text{ for } (a,b) \in Q\} \tag{A.4}$$

A.2. Hole filling operator

The operator used to fill the holes of the image, i.e. to remove background pixels inside foreground objects that result at the end of thresholding, requires, beside the original image $f(x,y)$, a marker image $f_m(x,y)$ defined as:

$$f_m(x,y) = \begin{cases} 1 - f(x,y) & \text{if} \quad x = 0 \vee x = N-1 \vee y = 0 \vee y = M-1 \\ 0 & \text{if} \quad x \in [1, N-2] \wedge y \in [1, N-2] \end{cases} \tag{A.5}$$

The operator is defined by means of a iterative procedure which uses an auxiliary succession of images W_i as follows:

1. initialize W_1 to F_m
2. calculate $W_{k+1} = (W_k \oplus I) \cap F^c$
3. if $W_{k+1} \neq W_k$ repeat step 2
4. the image with filled holes is W^c_{k+1}

A.3. Identification of regions

In a binary image, a foreground pixel is has value 1 while a background pixel has value 0. The set $N_4(p)$ containing the four neighboring pixels of a foreground pixel p with coordinates (x,y) is defined as:

$$N_4(p) = \{(x+1,y), (x-1,y), (x,y+1), (x,y-1)\} \tag{A.6}$$

two foreground pixels p and q are said to be adjacent if $q \in N_4(p)$ (obviously in this case is also $p \in N_4(q)$). A path between pixels p_1 and p_n is a sequence of pixels $p_1, p_2, \ldots, p_n$ such that p_k is adjacent to p_{k+1}. Two pixels are connected if there exists a path between them. A region is a set of pixels which are connected (Gonzalez et al., 2004).

References

Anthoine, A., 1995. Derivation of the in-plane elastic characteristics of masonry through homogenization theory. International Journal of Solids and Structures 32 (2), 137–163.
Cavalagli, N., Cluni, F., Gusella, V., 2011. Strength domain of non-periodic masonry by homogenization in generalized plane state. European Journal of Mechanics A-Solids 30 (2), 113–126.
Cecchi, A., Sab, K., 2009. Discrete and continuous models for in plane loaded random elastic brickwork. European Journal of Mechanics A-Solids 28, 610–625.
Cluni, F., Gusella, V., 2004. Homogenization of non-periodic masonry structures. International Journal of Solids and Structures 41, 1911–1923.
Gonzalez, R.C., Woods, R.E., 2002. Digital Image Processing, second ed. Pearson Prentice Hall, Upper Saddle River NJ.
Gonzalez, R.C., Woods, R.E., Eddins, S.L., 2004. Digital Image Processing Using MATLAB. Pearson Prentice Hall, Upper Saddle River NJ.
Gusella, V., Cluni, F., 2006. Random field and homogenization for masonry with nonperiodic microstructure. Journal of Mechanics of Materials and Structures 1 (2), 357–386.
Hill, R., 1963. Elastic properties of reinforced solids: some theoretical principles. Journal of the Mechanics and Physics of Solids 11, 357–372.
Lombardo, M., Zeman, J., Šejnoha, M., Falsone, G., 2009. Stochastic modeling of chaotic masonry via mesostructural characterization. International Journal for Multiscale Computational Engineering 7 (2), 171–185 <http://arxiv.org/abs/0811.0972>.
Miller, S.L., Childers, D.G., 2004. Probability and Random Processes: With Applications to Signal Processing and Communications, second ed. Elsevier Academic Press, Burlington, MA, USA.
Mistler, M., Anthoine, A., Butenweg, C., 2007. In-plane and out-of-plane homogenisation of masonry. Computers and Structures 85, 1321–1330.
Pande, G.N., Liang, J.X., Middleton, J., 1989. Equivalent elastic moduli for brick masonry. Computers and Geotechnics 8, 243–265.
Sab, K., 1992. On the homogenization and the simulation of random fields. European Journal of Mechanics, A/Solids 11 (5), 585–607.
Sab, K., 1994. Homogenization of non-linear random media by a duality method. Application to Plasticity, Asymptotic Analysis 9, 311–336.
Sab, K., Nedjar, B., 2005. Periodization of random media and representative volume element size for linear composites. Comptes Rendus Mecanique 333, 187–195.
Šejnoha, J., Šejnoha, M., Zeman, J., Sykora, J., Vorel, J., 2008. Mesoscopic study on historic masonry. Structural Engineering and Mechanics 30 (1), 99–117.